"A SUMMARY OF THE OV1-19 SATELLITE DOSE, DEPTH DOSE,
AND LINEAR ENERGY TRANSFER SPECTRAL MEASUREMENTS"

Captain John T. Cervini

Technology Division
Air Force Weapons Laboratory

1. INTRODUCTION.

The purpose of the radiation research satellite, OV1-19, was to make simultaneous measurements of the biophysical and physical parameters in the near earth space environment; specifically, the Inner Van Allen Belt. This region of space is of great interest to planners of the Skylab and the Space Station programs because of the high energy proton environment, especially during periods of increased solar activity. Currently, data on these radiations for both manned and unmanned space systems is inadequate. Many physical measurements of charged particle flux, spectra, and pitch angle distribution have been conducted and are programed in the space radiation environment. Such predictions are not sufficient to accurately predict the effects of space radiations on critical biological and electronic systems operating in these environments. Some of the difficulties encountered in transferring from physical data to a prediction of the effects of space radiation on operational systems are due to the following reasons:

(a) Theoretical computations of dose and linear energy transfer at depth are not precise.

(b) Shielding and mass distributions are only approximate.

(c) The proton spectra at high energies in the Van Allen Belts and in solar flares are uncertain.

The experiments aboard the OV1-19 satellite were designed to obtain accurate dose rate, depth dose, and linear energy transfer (LET) measurements. Accurate dose rate predictions are critically dependent on knowledge of the radiation environment, the shielding distribution surrounding the dose point, and radiation transport calculations. Simultaneous measurements provide knowledge of the physical spectra and the resultant dose rate behind known shielding configurations. These data may then be used to evaluate the accuracy of the transport calculations.

2. DESCRIPTION OF EXPERIMENT.

OV1-19 was launched on 18 March 1969 into an orbit with an apogee and perigee of 250 and 3125 nautical miles, respectively. The inclination of the orbit was 105°. The satellite consisted of a cylindrical center section which served as the container for the scientific payload, two faceted solar domes, and satellite support systems housed under each solar dome. The domes serve as the substrate for the solar cells which provide the primary power source for the satellite. Most of the experiments were mounted through apertures on the outer surfaces to insure unobstructed views of the environment (Fig. 1). Two of the onboard experiments are discussed here. These are the tissue equivalent ionization chambers (TEICs) and the cellular absorbed dose linear energy transfer spectrometer (CADS).

The dose rates were measured by three spherical TEICs whose sensor walls and cavity media simulate the response of muscle tissue to all ionizing radiation (ref. 1). The chambers were constructed of 0.236 gm/cm^2 of conductive tissue equivalent plastic and were filled with a tissue equivalent gas composed of methane, carbon dioxide, and nitrogen (ref. 2). TEICs of this type have successfully flown on many unmanned research satellites (ref. 3-6). A complete description of the design theory, fabrication, and calibration of these instruments can be found in reference 7. A typical TEIC sensor is shown in Fig. 2.
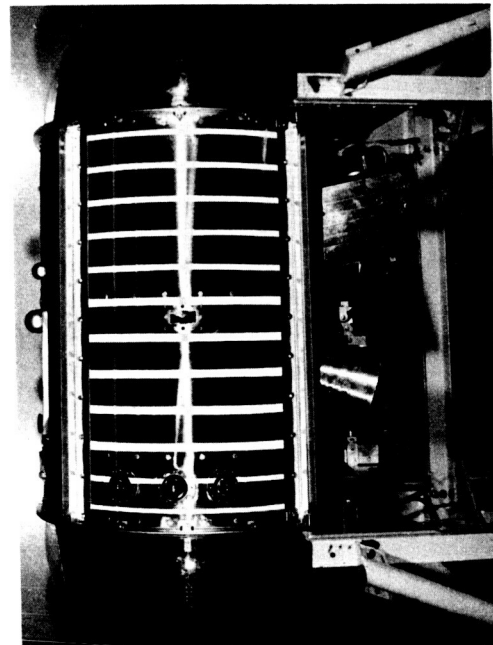

FIGURE 1. THE OV1-19 SATELLITE

The CADS instrument uses the scintillation method of detection to obtain its measurements. The sensor consists of a flat plate of NE-102 scintillating material attached to a lucite light pipe, which is in turn connected to a photomultiplier tube. The photomultiplier electrical responses are sorted and read out into various dE/dX channels, which are then processed in the analyzer (See Figs. 3 and 4). NE-102 scintillating material was used as a detector, since it closely approximates muscle tissue atomically and is readily adaptable for space flight application. It was machined into a flat plate 50 microns thick to approximate the path length across a human cell.
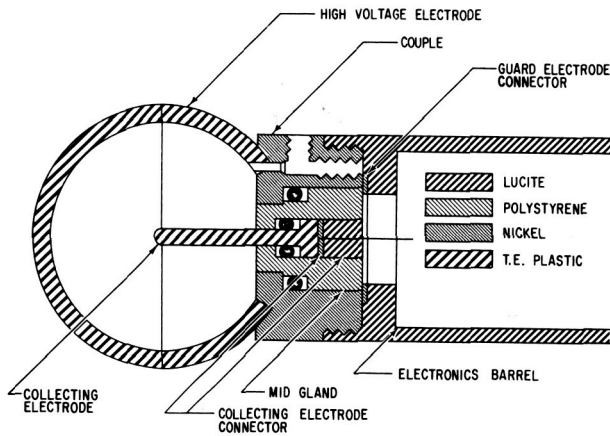

Figure 2   Tissue Equivalent Ionization Chamber Sphere and Barrel Assembly

TABLE 1.   TEIC CHARACTERISTICS

TEIC No.	Dose Rate Range (Rad/hr)	Shield Description (gm/cm^2)	Proton Energy Threshold (MEV)
3	.002 - 620	Bare	17.1
1	.005 - 150	5.0 Lucite	77.5
2	.01 - 47	12.0 Tungsten	86.6

15-99   1302-307   51°.

The dynamic ranges of the OV1-19 TEICs allow measurement of dose rates from 2.0 m rad/hr to about 620 rad/hr. As shown in Table 1, each sensor was adjusted to measure the range of expected dose rates for its shielding configuration. The shields on the OV1-19 instruments were much thicker than those on any TEICs previously flown. This design was chosen so that high energy proton sources (solar flare, Van Allen Belt, and cosmic radiations) could be carefully measured since they have a much wider energy range, and far less is known about their actions on biological matter. Also, both the USAF and NASA manned space vehicles of the 1970's will have enough average shielding to "stop" all but the most energetic protons. Thus, significant dose rates, and therefore any biological effects will be caused mainly by the higher energy protons which are merely degraded or interact by nuclear collision in a non-uniform manner with the shielding

The LET spectral data discussed in this report were obtained by the CADS instrument. LET is defined as the linear rate of loss of energy per unit length, locally absorbed, by an ionizing particle traversing a material medium. It is an important quantity in that it enables a more precise definition, on a microscopic scale, of the biological effect of energy deposition due to incident radiation.

The ionization rate of the particle (and hence the LET) changes with path length and particle energy as it traverses matter; so, it is necessary to determine the LET-depth profile rather than a single point determination. Fortunately, however, the change in ionization rate is small enough that the LET does not vary significantly over a few microns of path length, so that a measurement made in a path length comparable to a micron is representative of the LET of that particle at the cellular level. The CADS is designed to conduct these types of direct LET measurements.
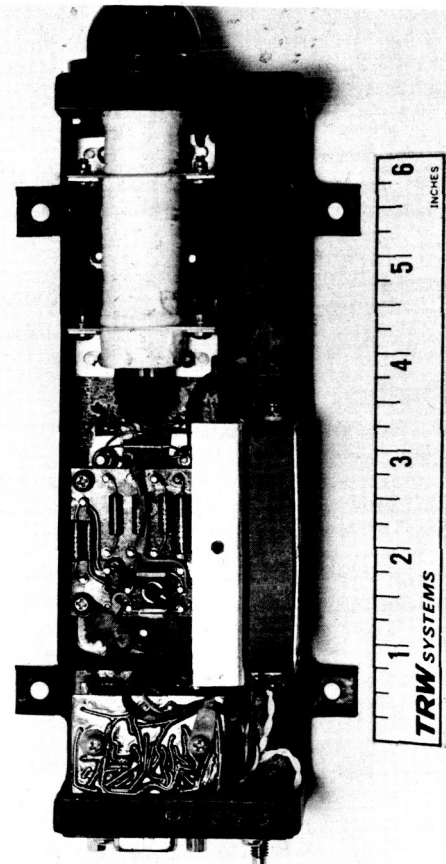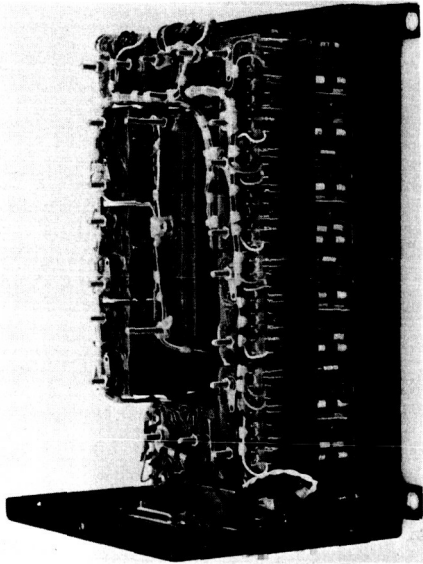

FIGURE 3.   CADS SENSOR

FIGURE 4. CADS ELECTRONICS

TABLE 2. CADS THRESHOLDS

Channel Number	Thresholds in MV	LET (kev/micron)
1	> 20	> .22
2	20-50	.22 - .55
3	50-75	.55 - .82
4	75-110	.82 - 1.22
5	110-160	1.22 - 1.86
6	160-230	1.86 - 2.9
7	230-335	2.9 - 4.7
8	335-480	4.7 - 8.5
9	480-700	8.5 - 19.0
10	700-1000	19.0 - 130
11	> 1000	> 130

/5 - 52   /302 - 307

The CADS analyzer unit contains signal processing circuits capable of producing the following measurements:

(a) An eight channel absorbed dose spectrum from approximately 130 kev/micron

(b) The number of events having LET greater than approximately 130 kev/micron

(c) Total events, which is a measure of all pulses exceeding the threshold of the lowest channel (0.2 kev/micron)

(d) Absorbed dose rate obtained by integrating the photomultiplier tube anode current for those pulses in the range of approximately 0.2 to 0.5 kev/micron.

TABLE 2 presents the values of the thresholds of all the CADS channels, and the corresponding LET values for each of the thresholds. More complete and detailed information on the CADS operation and design can be found in reference 8.

3. PROCEDURE FOR DATA REDUCTION.

Raw data tapes collected by ground stations were digitized to make them readable to an electronic computer, and to allow all noisy data to be edited. The data on the digitized tapes were then converted from the 36-bit-per-word format to 60-bit words, compatible with a CDC 6600 computer. Programs were then written to select the desired instrument outputs from the satellite telemetry format. Since the wave train format was Pulse Code Modulation (PCM), appropriate conversions from bits to volts were incorporated. The sub-commutator synchronization pulses were located and stripped off. The subcom information appeared on

one of the 256 main commutator words, and contained the instrument sensor electronics temperatures as well as instrument status indicators. Temperature information was provided for the calibration of the CADS log count-rate meters which are part of the analyzer circuitry. Calibration information was then programed to allow a further reduction from volts to physical units such as dose rate and LET count-rate for the TEICs and CADS, respectively. The physical data for each revolution was then written on magnetic tape for further analysis. Ephemeris information, which determines the satellite's position as a function of GMT, was provided directly by Ent Air Force Base, Colorado. Presently, the OV1-19 data is being merged to provide isodose rate and isocount rate versus B and L as well as versus longitude and latitude. The McIlwain parameters, B and L, (Ref. 9) are computed from Hendricks and Cain's 99 term expansion of the geomagnetic field (Ref. 10), using the ephemeris data as input.

The results given here are raw dose rates and count rates reduced from the OV1-19 satellite, since a detailed analysis of all the data has not yet been accomplished. The merging of all the satellite orbits is incomplete; however, some of the preliminary information obtained during increased solar activity is presented. Data on 120 orbits of the satellite indicate that both the TEICs and the CADS instrument were operating nominally until a malfunction occurred in the multicoder of the OV1-19 telemetry system, 11 months after launch.

No further contacts were made by ground command, and all data acquisition ceased.

4. PRESENTATION OF DATA.

Preliminary data reduction techniques have allowed a review of raw physical data results. The three TEIC sensors operated as planned, as did all the CADS channels. Some problems have occurred on channel two of the CADS instrument, and we are presently checking its outputs.

Most of the data presented here are from Revs. 265 and 2551, which were recorded during increased solar activity. On 12 April 1969, a proton event was recorded by the Solar Flare Forecast Network (SOFNET). The onset occurred at 0111Z and continued in intensification until midday of 13 April 1969, when peak values of proton fluxes were measured. SOFNET reported that the Vela 4 satellite obtained integrated proton fluxes of 200 counts/sec. above 25 MEV, and 33,000 counts/sec. in the range 3-20 MEV. OV1-19 recorded Rev. 265 approximately 2 hours after the peak of the event. Figures 5 and 6 are a time history of Rev. 265 for the TEIC sensors. Figure 7 gives the McIlwain B, L coordinates as a function of UT for the same Rev. Figure 5 shows that TEIC 1 reaches a peak dose rate of 4.5 rad/hr, and 4 minutes later, TEIC 2 peaks at 2.5 rad/hr.
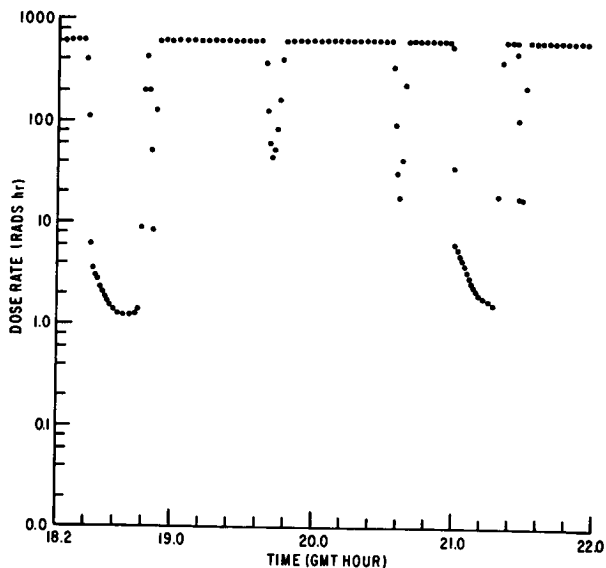

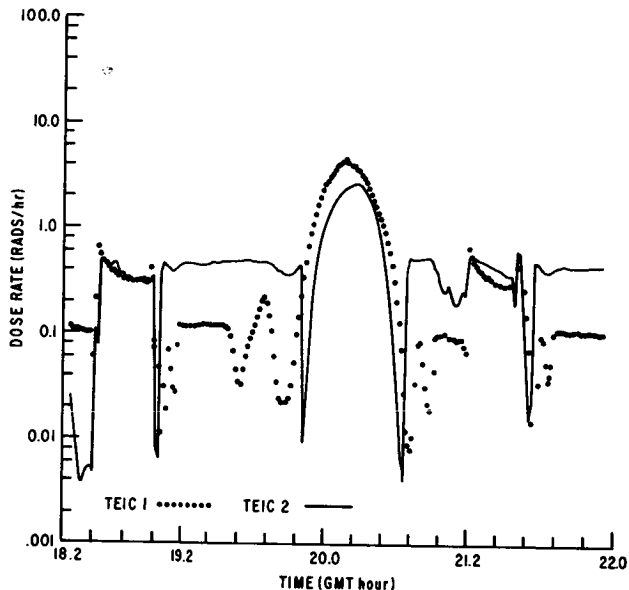Figure 6: TEIC 3 Dose Rate vs. GMT for REV. 265

Figure 5: Dose Rate vs GMT for REV. 265

At the time TEIC 2 recorded its peak dose rate, TEIC 1 was reading 3.5 rad/hr. These measurements were taken when OV1-19 was at a high northern latitude (75°N), at an altitude of about 720NM. Data from another revolution at the same latitude and altitude indicated that TEIC 1 and TEIC 2 recorded dose rates of 2.7 and 1.3 rad/hr, respectively. These measurements occurred during a quiescent solar period, when no precipitating solar particles were present in the earth's geomagnetic field. Rev. 265 shows an increase in dose rate for TEICs 1 and 2 of about 70% and 50%, respectively, due to the presence of solar flare particles at high northern latitudes. As expected, the TEIC 3 sensor saturated at 620 rads/hr during the greater portion of both orbits (Fig. 6). Since

there wasn't any shielding for this sensor, the threshold energy for protons, and to an extent electrons, was low allowing many of the lower energy particles to be absorbed in the chamber. Dose rate data during increased solar activity were also obtained on Rev. 2551 (Fig. 8). Note that both TEIC 1 and TEIC 2 initially peak at much higher values of dose rate than previously recorded. The maximum dose rate measured by TEIC 1 is now 9.2 rads/hr, and the maximum for TEIC 2 is 13.7 rads/hr. At this time, the satellite was at an altitude of 1673NM and a latitude of 33°N. Equivalent B and L values are .126 gauss and 2.17 earth radii (Fig.9). Figure 8 shows a second peak about 2 hours later. TEICs 1 and 2 now reach a maximum of 7.7 and 10.4 rads/hr, respectively. At the time of these measurements, OV1-19 was at an altitude of 3087NM, a latitude of 47°S, and a longitude of 309°E. Ten minutes earlier the satellite had reached its apogee (3125NM) at 37°S, 316°E. This indicates that the second peak of dose rate data was probably obtained above the South Atlantic Anomoly. The third and fourth peaks of Figure 8 are merely a repetition of the first two peaks at a later time in the orbit. Data was also reduced but not merged for a number of other orbits that occurred during solar flare events. The solar flare of 11 April 1969 was preceeded by a ground level neutron event that took place on 30 March 1969. This event was not recorded by our instruments; however, dose rate information was recorded 10 days after the event that were higher than the peaks of Rev. 265. TEICs 1 and 2 showed peak dose rates of 6.3 and 5.7 rads/hr for Rev. 223 which was obtained during the early hours (UT) of 11 April 1969, just prior to the April proton flare. The maximum dose rates measured during this event were 5.6 and 6.0 rad/hr on 12 April 1969 (Rev. 240). The closeness of the measurements tend to indicate that both sets of values are due to the same event. During the interval 19-21 November 1969, a class 2B solar flare was observed and on 14 December 1969 a class 3N
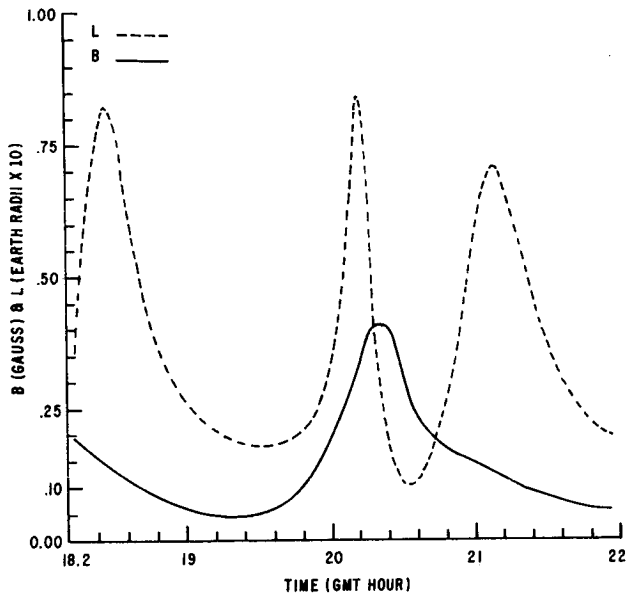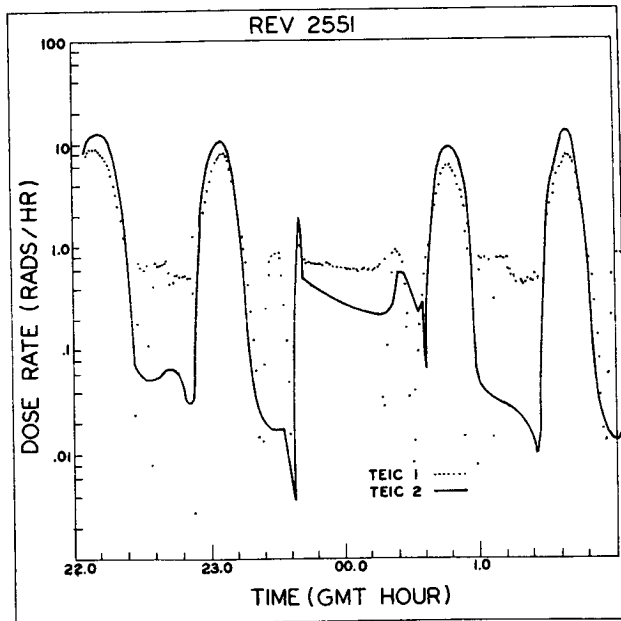
Figure 7: B, L vs. GMT for REV. 265

FIGURE 8: DOSE RATE vs. GMT for REV. 2551

behind relatively large amounts of shielding during solar flare events. This indicates that the radiation spectrum in the near earth space environment was hardened due to an influx of protons with energies greater than 70 MEV.

TABLE 3. MAXIMUM TEIC DOSE RATES

Rev. No.	Date	TEIC 1 Max. Dose Rate*	TEIC 2 Max. Dose Rate*	
	3/30/69			Ground Level Neutron Event
208	4/9/69	5.9	5.2	
222	4/10/69	3.2	1.3	
	4/11/69			Solar Flare Event
223	4/11/69	6.3	5.5	
240	4/12/69	5.6	6.0	
249	4/13/69	3.9	2.4	
265	4/15/69	4.4	2.6	
276	4/16/69	4.2	1.6	
296	4/18/69	4.3	1.7	
---	11/19/69 to 11/21/69			Class 2B flares
2308	11/19/69	12.3	10.9	
2318	11/20/69	8.0	10.4	
2327	11/21/69	7.6	8.6	
2369	11/25/69	8.4	8.7	
2377	11/26/69	8.3	9.7	
2393	11/28/69	9.0	9.7	
2395	11/28/69	8.5	10.1	
	12/14/69			Class 3N flares
2551	12/15/69	9.2	13.7	
2555	12/15/69	7.0	10.3	
2564	12/16/69	7.7	10.1	
2572	12/17/69	6.9	10.1	

*Rads/hr

The LET spectrum measured by CADS did not show an equivalent enhancement in all channels during solar flare events. Channel 1 recorded total events above a threshold of 20 MV, which corresponds to all particles having an LET greater than .22 kev/micron. Channel 2 measured the dose rate by integrating the photomultiplier tube anode current for those pulses in the range of approximately 0.2 to 0.5 kev/micron. Channels 3 to 11 actually measure the LET spectrum, and they are our main concern. They correspond to LET channels 1 through 9. The LET outputs for Rev. 265 are given in Figures 10 through 14. Note that LETs 3 through 9 each show a well defined count rate peak which corresponds to the peak dose rates for TEICs 1 and 2 (Fig. 5). This indicates that the energy deposited per unit path length increases as the dose rate increases. However, we do not observe an equivalent peak for LET channels 1 and 2 (Fig. 10). In fact, the count rate has decreased considerably to 5 counts/sec. This may mean that we are observing a shift in the LET spectrum to higher channels due to flux increases of high energy particles. A different orbit yielded a similar pattern of behavior for these two channels. However, in reducing the LET data for Rev. 2551, channels 1 and 2 did correspond to the TEIC dose rate peaks. Further analysis is needed to correct this discrepancy. TABLE 4 shows the peak count rates for each of the LET channels. The number of counts

flare took place. The dose rates for Rev. 2551 were obtained during the latter event. TABLE 3 summarizes the peak TEIC dose rates for orbits of data that occurred during the time of the four solar flare events mentioned above. Since the duty cycle of the satellite prevented continuous coverage of the sun's activity, there are many orbital gaps between the significant events. Therefore, definitive statements concerning the contribution of solar particles to the peak dose rates cannot be made at this time. The movement of apogee and perigee through the Van Allen Belts certainly has some effect on these measurements. The TEIC 1 and 2 results show that a considerable dose is received

TABLE 4

CADS LET Channel	LET Range kev/micron	Peak Count Rate
1	.55 – .82	–
2	.82 – 1.22	–
3	1.22 – 1.86	525
4	1.86 – 2.9	475
5	2.9 – 4.7	185
6	4.7 – 8.5	135
7	8.5 – 19.0	95
8	19.0 – 130	55
9	> 130	450

Figure 10: LET 1 & 2 (CADS Channel 3 & 4) for REV. 265

decreases monotonically for each succeeding channel, except for LET channel 9 which records the count rate for particles with LET greater than 130 kev/micron. For the greatest portion of a typical orbit of data, the largest number of the counts occur in channels 1 and 2. This indicates that most of the particles sampled have LETs in the range .55 – 1.22 kev/micron. Channels 3 and 4, with LET ranges of 1.22 – 1.86 and 1.86 – 2.9 kev/micron respectively, record the next highest average count rate. Channel 9 also measures a significant number counts, and they are normally of the order of the count rate of channel 3.
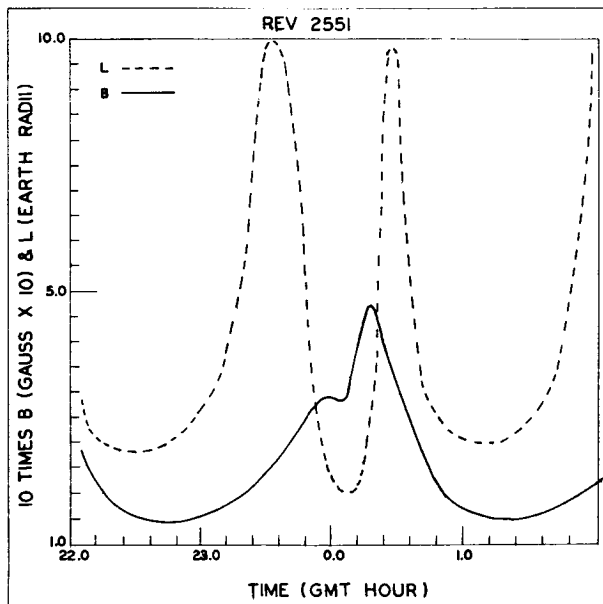
5. CONCLUSIONS.

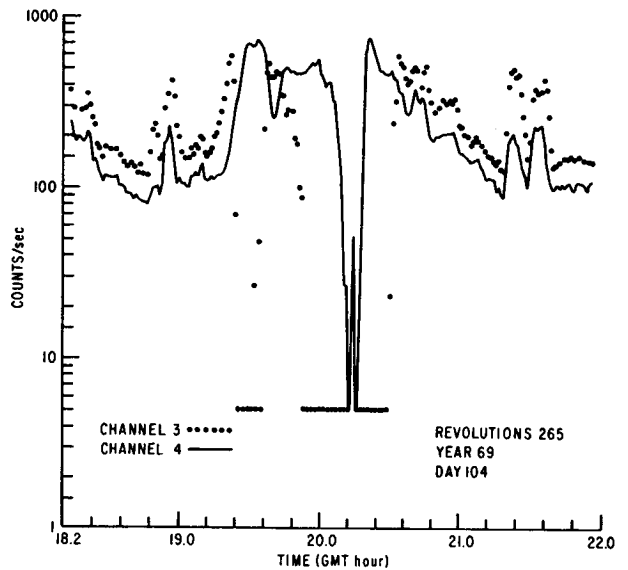The TEICs aboard OV1-19 show that a considerable dose rate can be expected even behind shielding whose cutoff energy is 70 MEV or higher. Most of this dose occurs due to solar flare radiation. A typical manned spacecraft provides a large amount of shielding in excess of 1.0 gm/cm^2 and the bone marrow and other vital organs are generally shielded by an additional 2.5 gm/cm^2 of surrounding tissue. Therefore, protons of high energy (> 60 MEV) are the dominant hazard to man in space. Doses from solar flares occur mainly over the polar regions. The earth's magnetic field masks out the solar flare protons almost completely in non-polar regions, where most of the Skylab missions will occur. However, if the rigidity of a flare is great enough, then the radiation belts may only partially mask out the solar flare radiation at altitudes of concern to earth orbiting manned vehicles. Also, many missions in the near future will take man outside the protection of the earth's geomagnetic field, where he will be more susceptible to the presence of a high proton environment. And, there is a great need for a more accurate description of that portion of the environment.

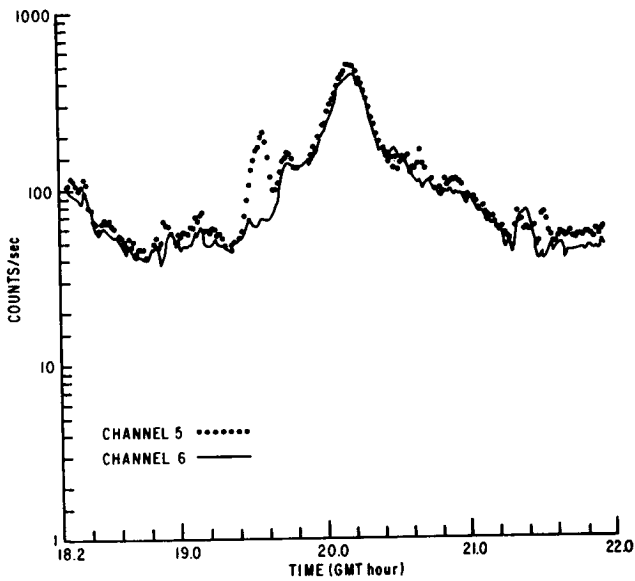FIGURE 9: B, L vs. GMT for REV. 2551

Figure 11:   LET 3 & 4 (CADS 5 & 6) vs. GMT
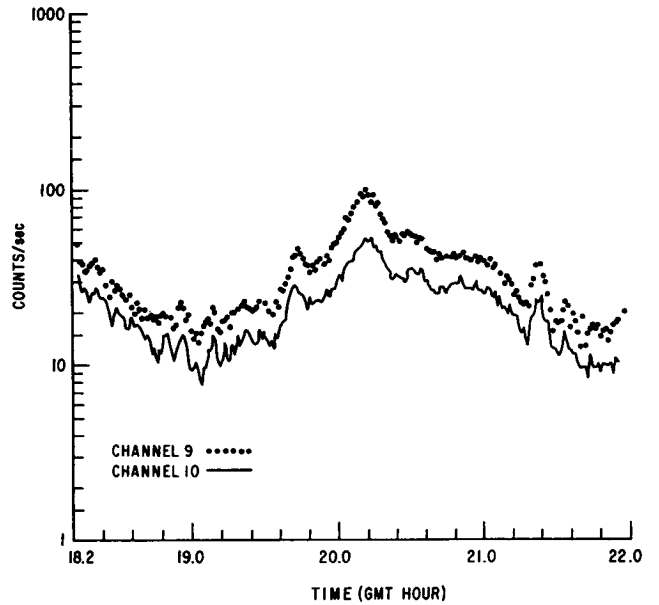

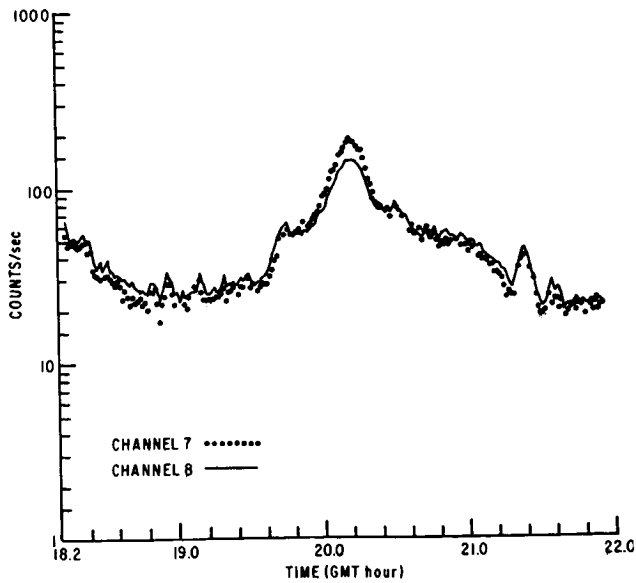Figure 13:   LET 7 & 8 (CADS 9 & 10) vs. GMT

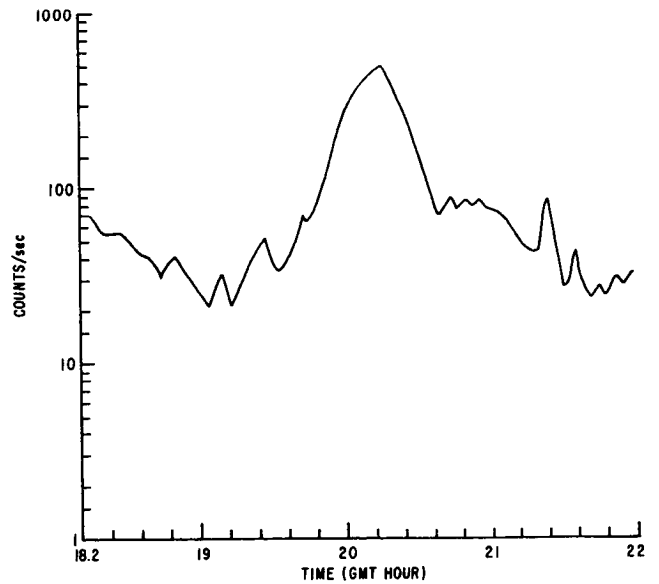Figure 12:   LET 5 & 6 (CADS 7 & 8) vs. GMT

Figure 14:   LET 9 (CADS 11) vs. GMT

REFERENCES

1. Schneider, M.F., _Advanced Spaceborne Dosimetry Instrumentation_, WL-TDR-64-96, AF Weapons Laboratory, December 1965.

2. Schneider, M.F., _Calibration of Dose Measuring Ionization Chambers Using High Energy Proton Beams_, WL-TR-66-30, AF Weapons Laboratory, 1967.

3. Trafton, L.M., _OV1-12 Dose Rate, Spectral and Flux Measurements_, AFWL-TR-69-104, AF Weapons Laboratory, January 1970.

4. Thede, A.L., _OV3-4 Dose Rate and Proton Spectral Measurements_, AF Weapons Laboratory, January 1969.

5. Fortney, R.E., _Flight Experiment Shielding Study (FESS) Satellite Data Analysis_, AFWL-TR-68-108, AF Weapons Laboratory, April 1969.

6. Janni, J.F., and Holly, F.E., "The Current Experimental Approach to the Radiological Problems of Spaceflight," Aerospace Medicine 40, December 1969.

7. Schneider, M.F., _An Active Dosimeter System to Measure Energy Deposition and Charged Particle Spectra of High Energy Inner Van Allen Belt, Solar Flare, and Galactic Cosmic Protons on Manned Spacecraft_, AFWL-TR-70-29, AF Weapons Laboratory, August 1970.

8. Chapman, M.C., _Development of a Cellular Absorbed Dose Spectrometer_, AFWL-TR-69-76, AF Weapons Laboratory, December 1969.

9. McIlwain, C.E., "Coordinates for Mapping the Distribution of Magnetically Trapped Particles," _Jour. Geophys. Rsch._, 66, p. 3681, 1961.

10. Hendricks, S.J., Cain, J.C., "Magnetic Field Data for Trapped Particle Evaluation," _Jour. Geophys. Rsch._, 71, p. 346, 1966.